Dose Reduction for Historical Books Digitization by 3-D X-Ray CT

Daniel Stromer[1], Vincent Christlein[1], Yixing Huang[1], Patrick Zippert[2], Eric Helmecke[2], Tino Hausotte[2] and Andreas Maier[1]

[1]FAU Erlangen-Nuremberg, Pattern Recognition Lab, Germany, e-mail: daniel.stromer@fau.de, vincent.christlein@fau.de, yixing.huang@fau.de, andreas.maier@fau.de

[2]FAU Erlangen-Nuremberg, Institute of Manufacturing Metrology, Germany, e-mail: patrick.zippert@fmt.fau.de, eric.helmecke@fmt.fau.de, tino.hausotte@fmt.fau.de

Abstract
Corruptions such as aging-processes or moisture make it often impossible to digitize historical books or scrolls with common digitization approaches. 3-D X-ray CT is a non-destructive method which can provide a look inside those documents. Current CT scans use a full-circle trajectory with a large number of projections and high exposure times. However, there are historical goods that may suffer from high radiation dose. In this work, we present an evaluation of a 3-D X-ray CT scan with three reduced projection sizes reconstructed with four common algorithms compared to the mentioned high dose approach. For our experiments, we used a book with 22 pages and a leather cover. Every page has writings made with iron gall ink. We show that we can reduce the number of projections by at least 85 and up to 92.5 percent without severe loss of information on the book's writings. The reconstructed volumes are compared with regard to common similarity measures as well as visual outputs of a selected 2-D mapped page.

Keywords: 3-D X-ray CT, Historical Document Analysis, 3-D Reconstruction, Iron Gall Ink, Iterative Reconstruction

1 Introduction

When digitizing historical books, the current state-of-the-art approach is to place the book into a scan robot and photograph it page by page. However, this method can not be used if the book suffers from aging-processes or other damages such as moisture. Typically, those damages make it impossible to turn pages at all without further destruction. More and more, methods are proposed that scan such documents in a non-destructive manner providing a 3-D volume where the writings can be investigated by experts.

One method that can provide a look into the closed book is 3-D Terahertz imaging [1]. This technique does not expose ionizing radiation to the document, however, it has a limited penetration depth and resolutions of about 0.4 mm^3 whereas pages can have thicknesses of les than 0.1 mm. Furthermore, it has not been tested for real historical documents so far. Historical books pose a different problem because they use ink made of metallic particles [2], and Terahertz waves are reflected by metal. A technique, which is gaining more and more importance in the field of document digitization is 3-D X-ray micro-CT. We showed in previous works, that common micro-CT systems can deliver good results by exploiting the different material characteristics of historical ink and paper [3,4]. The metallic particles in the ink allow to differentiate between writings and paper enabling to read a book that can not be opened anymore. Resolutions of micro-CT reach about 1 μm^3 or even lower. X-ray phase contrast is another approach that is capable of scanning such manuscripts [5]. However, this technique is not as widely accessible as micro-CT such that libraries would have to carry their documents to the measurement centers. The drawback the latter methods is that X-ray radiation can accelerate the aging of cellulose such that the state of the documents deteriorates when performing a scan [6]. If the document is already in a bad condition (e.g., burnt or moistured), this might be the only option to investigate the manuscript because the conservators can not separate the pages by hand anymore. However, there are also books where only pages are stuck together at the area of the book fold. Here, the restorer has to trade off the possible damage of the writings within the manual process. Our approach is based on a micro-CT scan because those systems are more mobile and could be set up in libraries.

Current micro-CT scans use a 360° full-circle scan acquiring a large number of projections (up to 2400) and high exposure times (up to a few seconds per projection) [7]. There are historical goods that may suffer from the applied radiation dose. Another challenge is the thickness of the pages (about 80 μm for our book) which are squeezed together such that the reconstruction gets inaccurate and the pages can not be easily separated. Fig. 1 shows a reconstructed book slice orthogonal to the book cover. While the upper and lower pages are approximately even (green box), the pages in the center are wavy and sometimes stuck together (orange box). To counter this, the reconstructed volume has to have a high resolution. 3-D micro-CT scans for manuscripts are performed with a rather small radiation energy, which makes it possible to differentiate the rather small metallic ink particles from the cellulose. However, this increases the

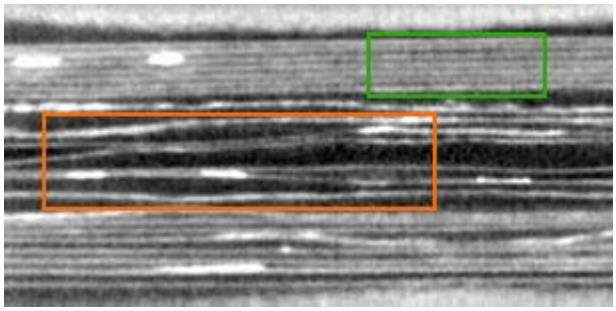

Figure 1: Reconstructed 3-D volume slice orthogonal to the front cover of the book. The green box denotes pages that are approximately even and can be investigated easier than the wavy pages denoted by the orange box.

noise levels dramatically. Reducing the applied dose by scanning with a low radiation energy and reduced projection size is a well-known technique in medical imaging known as the ALARA principle (as low as reasonably achievable) [8] which also holds for the digitization process. In medical imaging, not full-circle but so called short scans are the state-of-the-art for cone-beam CT scans [9]. This method makes use of the fact that a reconstruction is possible when acquiring projections of half a full-circle plus fan-angle (or even less [10]) reducing the number of projections by about a half. When performing low dose scans with a small number of projections, the commonly used reconstruction algorithms for cone-beam CT can get inaccurate and the signal-to-noise ratio decreases. Therefore, different reconstruction algorithms, e.g. iterative approaches, can help to reduce noise while simultaneously preserving the signal.

In this work, we compare short and full-circle scans with different numbers of projections with a scan having a high number of projections. As the reconstruction result with a small number of projections gets more inaccurate, we evaluate the effectiveness of four different reconstruction techniques on the acquired data – one analytical and three iterative approaches. We evaluate the methods with common statistical measurements as well as visual inspection of extracted pages and writings. We show, that reducing the projection size by 85 to 92.5 percent still leads to good results when applying appropriate algorithms.

2 Materials and Methods

2.1 The Scanned Book

The aim of this paper is to investigate how much the applied dose can be reduced for a real document while keeping all writings of the book readable. Therefore, we can not run our experiments with real documents but had to build a model that consists of the same components as the manuscripts that we want to scan in later scans. The book used for this experiment has 22 pages of different papers and a leather cover (Fig. 2). As paper we used hand-made paper (14 pages), parchment (four pages) and papyrus (four pages). For writing the letters we used iron gall ink. The ink consists of metallic particles ($FeSO_4$) making it possible to differentiate it from the paper when using X-ray scans. This kind of ink has been widely used since the Roman Empire until present. Many important historical writings such as the 'Declaration of Independence' were written with as it is indelible [2]. The material of the paper and the leather is considered to be cellulose. The size of one page is about $4 \times 4 \times 0.1\ cm^3$ and writings have a size ranging from 0.5 to 1 cm.

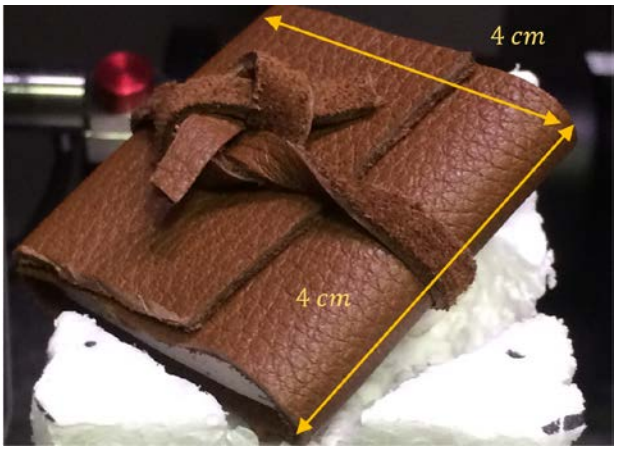

Figure 2: The self-made book consisting of leather, paper and iron gall ink.

2.2 The 3-D Volumetric Scans

Initially, we performed a full-circle cone-beam geometry 3-D X-ray CT scan with 60 kV, 300 μA and 1.5 s exposure time. The source-to-rotation-axis distance was set to 42 cm whereas the the source-to-detector distance to 48 cm. The detector has a pixel size of 44 μm and we cropped the projection size to $960 \times 256\ pixel$. We acquired 800 projections over 360° where the book was placed in the scanner such that the front cover was orthogonal to the rotation axis as shown in Fig. 3. Thus, cone-beam artifacts are reduced and a balanced penetration length of the beams was achieved [3].

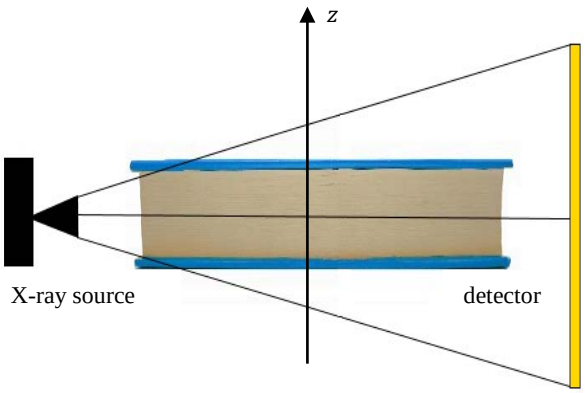

Figure 3: The book is placed in the scanner such that the front cover is orthogonal to the rotation axis z.

Apart from the full-circle scan, medical imaging utilizes another kind of trajectory. Because after 180 degrees of scanning most of the data beyond this point is redundant, the projections can be reduced to that point. As the cone-beam technique is based on fan-beam geometry, the fan angle has to be considered. We assume that the data is complete after 180° plus 2α, with α denoting the fan angle. As the fan angle of our system is 8.4° and we consider a sufficient buffer, we chose a rotation angle of 216° for our experiments.

To decrease the number of projections for our evaluation, we excluded the unnecessary projections from the dataset and compared the results with the complete dataset. The reference measurement is a full-circle scan with 800 projections. To compare also low-dose full-circle scans with short scans, we first chose a reduced full-circle scan with 200 projections. For the short scan, we picked out 120° and 60°. Table 1 shows all scan trajectory settings including the angulation angle which denotes the step width for the projections in degrees.

Scan Mode	Full Circle	Full Circle	Short Scan	Short Scan
Number of projections	800	200	110	60
Angulation step width	0.45°	1.8°	1.8°	3.6°

Table 1: Tested scan trajectories including two full circle scans and two short scans with decreasing number of projections.

2.3 The 3-D Reconstruction Algorithms

2.3.1 Analytic 3-D CT Reconstruction

Commonly, 3-D reconstructions in non-destructive testing are calculated by using the Feldkamp, Davis and Kress (FDK) algorithm [11] extended by pre-processing and post-processing filters such as ring artefact correction or scatter correction. The FDK is an analytical reconstruction approach solving the problem of the Radon Transform problem by performing three steps – cosine and ramp filtering followed by backprojection. This kind of reconstruction is exact if Tuy's condition holds [12] stating that every plane that intersects the object-of-interest must contain a cone-beam focal point. When running a short scan with 216°, we have a subset of redundant data because some rays are observed twice. As we know where those rays are located, we can weight them by using Parker Weights [9] to receive a correct result. This approach is computationally fast and delivers good results for scans with a high number of projections, however, when decreasing them the output of the FDK can get noisy and corrupted by artifacts.

2.3.2 Iterative 3-D CT Reconstruction

In medical imaging, so called iterative reconstruction techniques are getting more and more important because they can deal with the low radiation energy and the small projection size. In this work, we evaluate three iterative reconstruction approaches. Those methods solve the inverse radon transform problem by minimizing an objective function. An example for an unconstrained objective function is defined by the Sum of Squared Differences (SSD) measure between the original projection values and the projected current image:

$$\text{minimize } \|A\, f(r) - p\|_2^2 \tag{1}$$

$f(r)$ is the value of voxel $r = (r_1, r_2, r_3)$ in the reconstructed volume f whereas p denotes the measured raw projection data. $A\, f(r)$ is the system of linear equations with Radon transform A. An initially estimated volume is forward projected, the projections are compared to the original ones, corrected and backprojected again. This process is repeated until a maximum number of iterations is reached or the difference of the corrected and the original volume is smaller than a threshold. With every step, the noise is decreased and aberrations are corrected. This approach enables the decoupling of the spatial resolution from the image noise [13].

A. Simultaneous Algebraic Reconstruction Technique

A common iterative approach is the Simultaneous Algebraic Reconstruction Technique (SART) [14,15]. Within SART, the volume is updated simultaneously after all projection rays have been processed. After estimating an initial volume, the orthogonal projections to the hyperplanes are calculated by back projection and their centroid is stored, which is the new starting point for the next iteration. The update rule for SART is

$$\hat{f}_i^{\nu+1} = \hat{f}_i^{\nu} + \beta \sum_{k \in s(\nu)} \frac{1}{\sum_j (A^\top)_{i,j}^k} (A^\top)_{i,j}^k \frac{\sum_i A_{j,i}^k \hat{f}_i^{\nu} - p_j^k}{\sum_i A_{j,i}^k}, \nu \in [0, N_{Sub}[. \tag{2}$$

Here, j denotes the index of one projection element and i the index of volume voxel r. k denotes the index of a subset's projection. This yields to the Radon transform $A_{j,i}^k$ of projection k mapping f on p_k. We split the projection data into N_{Sub} subsets where ν denotes the current subset. $s(\nu)$ denotes the number of projections inside a subset while β denotes a relaxation parameter used to control the convergence speed of the minimization. We set N_{Sub} to the total number of projections leading to a subset size $s(\nu)$ of 1 which means that every projection is handled separately. As initial volume, one can either just set all voxels to zero or use the FDK reconstruction result. It has been shown that this corrects streak artifacts in high contrast areas faster than the zero-filled volume [16]. Hence, for this work, we used the FDK result as initial volume.

B. Penalized Weighted Least Squares Reconstruction

The second iterative reconstruction approach is a model based iterative reconstruction which uses statistical weights trying to model the polyenergetic X-ray source spectrum and the measurement nonlinearities caused by energy-dependent attenuation [17]. For our experiments, we chose the penalized weighted least squares (PWLS) cost function [18]:

$$\text{minimize } \frac{1}{2} \sum_{i=1}^{I} w_i (Af - p)_i^2 + h(f) = g(f) + h(f) \tag{3}$$

Here, $f \in \mathbb{R}^J$ denotes the volume to reconstruct, $p \in \mathbb{R}^I$ is the raw projection data, $A \in \mathbb{R}^{I \times J}$ is the CT's geometry matrix mapping volume f to the projection p. $w \in \mathbb{R}^I$ denotes the least squares weight accounting for a certain projection's noise level calculated by the variance of p. $g(f)$ is the data fidelity term, which commonly produces sharp but noisy results. For this approach, we used the Algebraic Reconstruction Technique (ART) algorithm [19] to increase the data fidelity. To get rid of the noise, a penalty function $h(f)$ is added for smoothing the output (Eq. 4).

$$h(f) = \beta \sum_{j=1}^{J} \sum_{k \in N(j)} \Psi(f_j - f_k), \tag{4}$$

β is a tunable control parameter, $N(j)$ is the neighborhood of a pixel j, and $\Psi(f)$ is the Huber penalty function defined as

$$\Psi(\mathrm{t}) = \begin{cases} \mathrm{t} - \delta/2, & \text{if } t \geq \delta \\ t^2/2\delta, & \text{if } t < \delta \end{cases}. \tag{5}$$

Here, δ denotes the limit where the loss function changes from linear to quadratic while t is the input function. The control parameter β has a large influence on the reconstruction results. A too small value might not suppress the noise whereas too high values can lead to over blurring of the volume [20]. Again, we use the FDK reconstruction as initial volume.

C. Weighted Total Variation Reconstruction

The last algorithm is based on the compressed sensing theory stating that it is possible to reconstruct a function with a high probability with less samples than required by the Nyquist-Shannon theorem if most entrys of its sparsifying transformation are zero. Within 3-D reconstruction, this means that we can reduce the number of projections and still obtain good results by exploiting sparsity in a specific domain [21]. In medical imaging, a commonly used regularizer to achieve sparsity is the Total Variation. The optimization can be formulated as follows:

$$\text{minimize } \|f\|_{wTV} \quad \text{subject to} \quad Af = p \tag{6}$$

$$\|f\|_{wTV} = \sum_{x,y,z} W_{x,y,z} \left\|(\nabla f)_{x,y,z}\right\| = \sum_{x,y,z} \frac{1}{\left\|(\nabla f)_{x,y,z}\right\| + \delta} \left\|(\nabla f)_{x,y,z}\right\| \tag{7}$$

The term $\|f\|_{wTV}$ has to be minizimed subject to the data fidelity term $Af = p$. For our work, we used the SART algorithm to increase data fidelity. The TV regularization is weighted by a matrix W which should enhance sparsity in the gradient domain leading to the weighted TV (wTV) algorithm [22]. Here, δ is a control parameter influencing the resolution of the volume and x, y, z are voxel indices. $(\nabla f)_{x,y,z}$ denotes the gradient of the volume in the given direction according to $(\nabla f)_{x,y,z} = \left(\nabla_x f_{x,y,z},\ \nabla_y f_{x,y,z},\ \nabla_z f_{x,y,z}\right)$. The SART reconstruction and wTV minimization are repeated N times or until convergence. For the wTV minimization step, M gradient descent iterations are performed by applying a backtracking line search. To retain a convex problem, we assume W to be constant for all M iterations and update the matrix afterwards. To further reduce the projection number, this algorithm can be extended by regarding a larger neighborhood instead of only two voxels [23]. TV algorithms are well suited for piecewise constant objects which is the case for our book's geometry. As this algorithm uses SART, we also use the FDK reconstruction as initial volume.

2.4 Evaluation Measures

For all calculations, we used the CONRAD framework [24] for cone-beam reconstructions. The scan parameters described in section 2.2 lead to a volume size of $768 \times 768 \times 256\ voxels$ with an isotropic voxel size of $50\ \mu m^3$. Furthermore, we restricted the reconstruction to a circular area with $r = 384\ pixel$ to reduce truncation artifacts and we normalized all images to an intensity range of $[0,1]$. All reconstructions were processed on a NVIDIA Titan Xp GPU for reducing computation times to a minimum.

We compared all performed scan reconstructions to the original reconstruction with 800 projections. As similarity measurement, we use the root-mean-square-error (RMSE) and the structure-similarity-index-measure (SSIM) of the complete volumes. A low RMSE value states that the two compared volumes differ only slightly while the SSIM is 1 if the outcomes are completely equal and 0 if they completely differ. The third measure is the volumes peak-signal-to-noise-ratio (PSNR). The greater the PSNR, the more similar the volumes are. Furthermore, we compare the scans with respect to computation time.

Due to the high resolution of the volume, it is hard to investigate single pages. The pages are wavy, rather thin and sometimes stuck together. In previous works, we developed a fully-automatic page segmentation algorithm [25,26] which is capable of virtually flattening and 2-D mapping the pages such that a visual investigation of each single page is possible. The algorithm binarizes the volume into page or air. Afterwards, corrupted areas are closed and smoothed iteratively until convergence and the pages are mapped to 2-D. Finally, the user can investigate all pages and further post-process them if needed. The computation time for applying the algorithm was around three minutes per volume.

Lastly, we evaluate the separability of the pages for the high dose scan of all reconstruction algorithms. Therefore, we compare an intensity plot along a line over all pages as shown in Fig. 4. If two pages are stuck together, overblurring by the algorithm can cause that they can not be separated anymore. If the output is too noisy, edges will appear in air gaps. The best algorithm will be detected by visual inspection of the plot.

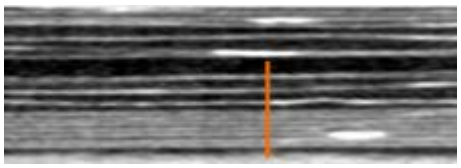

Figure 4: The plot along the orange line is compared for all reconstruction algorithms.

3 Results

Before running the reconstructions, appropriate parameters for the iterative reconstructions had to be configured. Table 2 shows the configured parameters. For a better comparability, we set the number of iterations for all approaches to 30.

Algorithm	$Iterations$	β	δ	M
SART	30	0.8	n.a.	n.a.
PWLS	30	0.01	0.001	n.a.
wTV	30	0.8	0.001	10

Table 2: Configured reconstruction parameters for the three iterative reconstruction approaches.

Table 3 shows the evaluation measures for all reconstruction algorithms applied to the reduced projection sizes. For all algorithms, we compared the reduced projection size with the 800 projection scan. This results in an optimal result for the similarity measurements of the high dose scan. As expected, reducing the projection size increases the error for all algorithms and decreases the computation time. In terms of computation time, the FDK reconstruction outperforms all iterative methods. When comparing only the iterative reconstructions, SART is the fastest method and PWLS the slowest. Within FDK and SART the computation time increases linear proportional to the projection stack size. SART and FDK lead to about the same similarity measurements which should be due to the FDK initialization of the SART algorithm. One can observe that the PWLS algorithm outperforms all other approaches. The full-circle scan with 200 projections has the best results, with the SSIM reaching approximately 1. The similarity for the 120 projection short scan is still very high. However, PWLS also has the highest computation time. The wTV approach also shows good results for all projection sizes and outperforms SART and FDK in terms of similarity measures with a SSIM of 0.93 for the 60 projection short scan.

Algorithm	Projections	RMSE	SSIM	PSNR	Time [s]
FDK	800	1	1	INFINITY	**91.5**
	200	0.0122	0.978	38.24	**20.7**
	120	0.0198	0.943	34.05	**12.9**
	60	0.0311	0.871	30.15	**7.6**
SART	800	1	1	INFINITY	432.6
	200	0.0124	0.979	38.40	108.1
	120	0.0196	0.941	34.04	193.0
	60	0.0313	0.872	30.13	96.5
PWLS	800	1	1	INFINITY	3105.7
	200	**0.0022**	**0.999**	**53.33**	765.2
	120	**0.0065**	**0.991**	**43.84**	1201.5
	60	**0.0110**	**0.975**	**39.14**	655.2
wTV	800	1	1	INFINITY	2256.8
	200	0.0091	0.987	40.84	1260.8
	120	0.0139	0.970	37.10	855.2
	60	0.0217	0.930	33.25	518.6

Table 3: Measures for the evaluated reconstruction algorithms with decreasing projection size. The volumes were compared with their respective 800 projection volume. For the similarity measures, the PWLS algorithm showed the best results. In terms of computation time, the FDK algorithm is the fastest algorithm, followed by SART, PWLS and wTV.

Another interesting observation can be seen in Table 4. Here, the 120 projection short scan was compared to the 800 projection FDK full-circle scan. While the FDK, SART and PWLS have about the same similarity measures, the wTV outperforms all other approaches. This result holds for all other decreased projection sizes, meaning that the reconstructed volume of the wTV is more similar to the high dose FDK scan than all other approaches' results. This verifies our assumption that with less projections, the FDK gets more inaccurate and applying appropriate iterative approaches leads to improved results.

Algorithm	FDK	SART	PWLS	wTV
RMSE	0.01983	0.01983	0.01977	**0.01486**
SSIM	0.94325	0.94325	0.93078	**0.96647**
PSNR	34.05	34.05	34.08	**36.56**

Table 4: Comparison between the state-of-the-art high dose FDK reconstruction (800 projections) and the 120 projection reconstruction for the three algorithms. The wTV has the highest similarity to the high dose scan.

Fig. 5 shows a photography of the original page-of-interest that we chose to investigate from the reconstructed volume where the height of the writings range from $1 - 1.5\ cm$. By applying the aforementioned page flattening and extraction algorithm, we extracted the page from the reconstructed volume and mapped it to 2-D for a visual investigation of the writings' visibility. Table 5 shows the received outputs for the reconstruction approaches (columns) and the decreased projection sizes (rows). With reduced projections, the noise increases. The writings are clearly visible in all projections, such that we can say, that even with only 60 projections (92.5 percent less dose), we are still able to read all writings. However, as a trade-off, we think that 120 projections might be a fair deal between increased noise and a dose reduction of about 15 percent. Although the PWLS algorithm has the best similarity measures, the output of the page is overblurred compared to the other algorithms. This is due to the fact that the similarity measures are highly sensitive to noise meaning that smooth results lead to better results. With respect to the results of Table 4 and the visual output, we conclude that the wTV algorithm shows the best results with the output being not overblurred.

Figure 5: Original page of the book model.

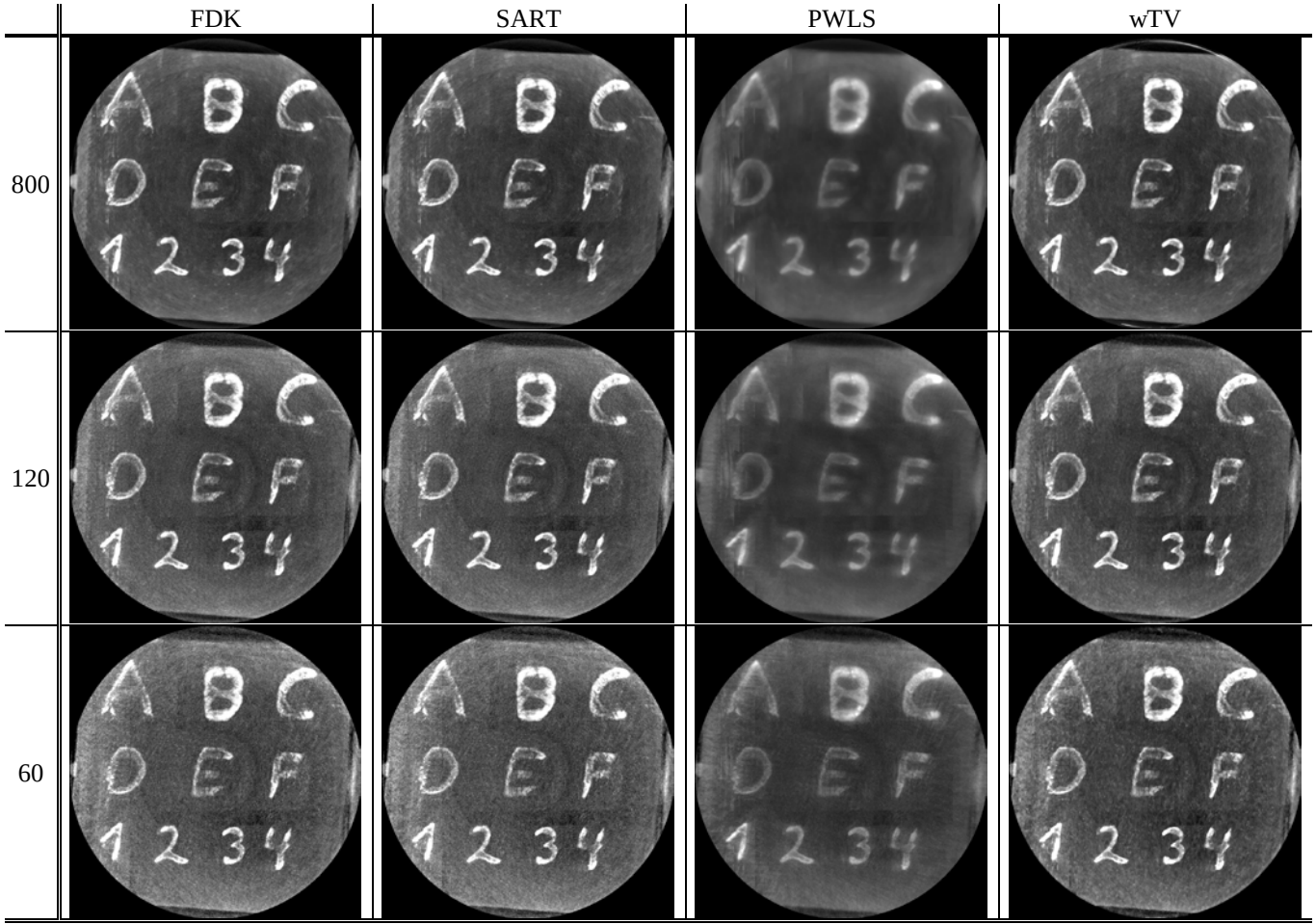

Table 5: The 2-D mapped pages for all reconstruction algorithms and three projection sizes. The top row shows the high dose scan, the center and lower row the short scans. FDK and SART show the same output, PWLS is overblurred while wTV shows the best visual output.

Finally, the separability of the pages was investigated. Fig. 6 shows the intensity plots along the line demonstrated in Fig. 4 for the high dose scan with 800 projections after applying the four reconstruction algorithms. Every peak denotes a page whereas the valleys denote air gaps. The first seven pages are made of paper ($z = [0, 45]$) whereas the last two are papyrus ($z = [46, 60]$). The overblurring of the PWLS (green) smoothes the curve too much such that the peak-to-peak amplitudes are very small. The difference between SART/FDK (red) and wTV (blue) is highlighted by the orange circles. For the wTV, the peak-to-peak

amplitudes are kept (left circle) while all pages of a certain material have about the same peak intensity. This does not hold for the FDK/SART approach. The right circle denotes an air gap which should be a smooth area. The wTV smooths this gap while the FDK/SART algorithm has a small local maximum that may be identified as a page.

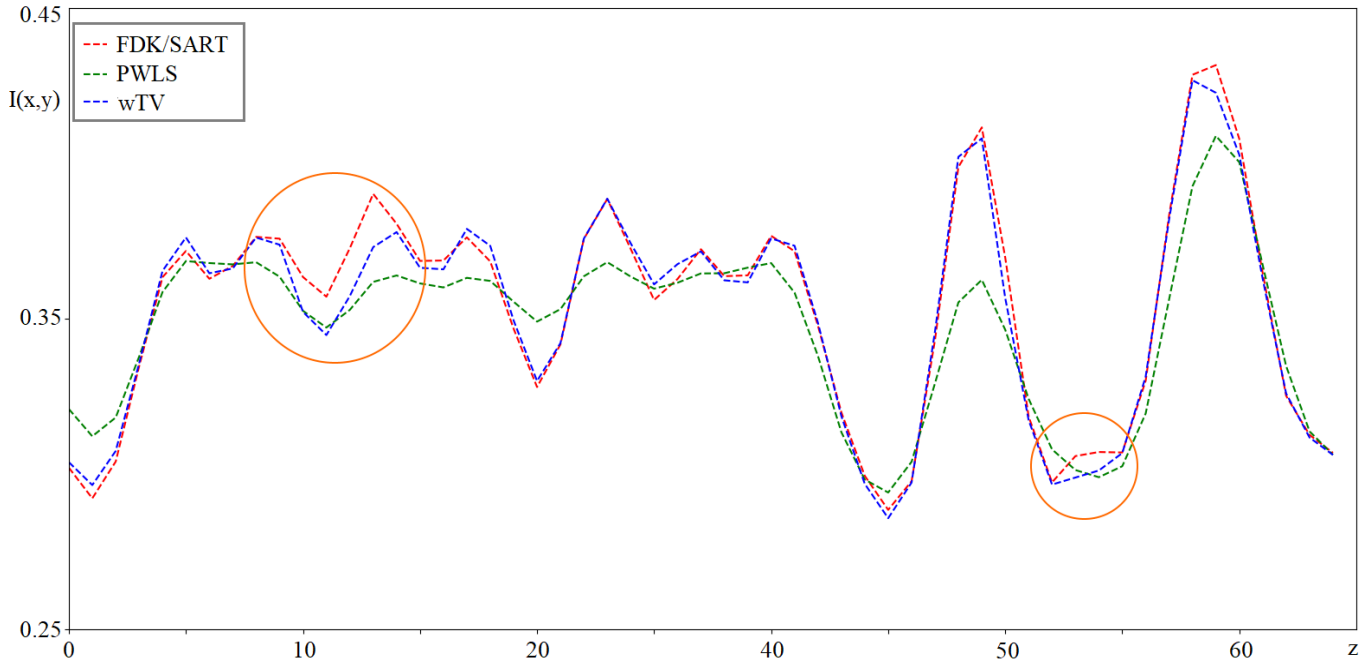

Figure 6: The intensity plot along a line (see Fig. 4) is shown for the reconstruction algorithms applied on the high dose scan with 800 projections. The first seven pages ($z = [0, 45]$) are made of paper while the right two pages are papyrus ($z = [0, 45]$). The PWLS curve is smoothed too much such that pages can not be separated easily. The wTV keeps the original structure but smoothes air gaps (right orange circle) and the peak intensities for a certain material are about the same (left orange circle) compared to FDK/SART.

4 Conclusion and Outlook

In this work, we evaluated how a decrease in the projection size of an X-ray micro-CT scan effects the accuracy of the 3-D reconstruction when using different reconstruction algorithms. Therefore, we performed a full-circle scan with 800 projections of a self-made book. Afterwards, we decreased the projection size stepwise and reconstructed the low dose volumes with four different reconstruction algorithms: FDK, SART, PWLS and wTV. The results of the low dose volumes were compared to their associated high dose reconstruction as well as to the high dose FDK approach, which is the current state-of-the-art method.

We showed that when using only 15 percent of the original projection data set, the image quality stays nearly the same for the wTV and PWLS reconstruction algorithm. The writings of the reconstructed and 2-D mapped pages were clearly visible and readable for all used projection sizes and algorithms. The output for all algorithms showed increased noise with reduced projection size. The PWLS achieved the best results when comparing it with its associated high dose scan, however, the images are overblurred. The good similarity measures of this approach can be explained by the fact that the measures are highly sensitive to noise and smooth outputs lead to better results. The wTV algorithm had good similarity measures and an improved noise suppression compared to FDK and SART. While the FDK had the lowest computation time (7.6 s for 60 projections), the slowest method was the PWLS (655.2 s). By further reducing the projection size to 60 projections (7.5 percent of the original scan), all writings were still visible, but the noise increased. Hence, we conclude that performing a short scan with 120 projections and applying wTV reconstruction leads to the best results for our tested object when we want find a trade-off between image quality and applied dose. Our result is supported by the fact that when comparing the results of low dose reconstruction with the high dose FDK reconstruction, the wTV outperforms the other approaches. In addition, the separability of the pages was enhanced with wTV because the peak intensities of the pages are at the same level and air gaps are smoothed compared to FDK and SART.

Our work demonstrates that we were able to dramatically reduce applied dose by reducing the projection size. Until now, historical documents are scanned with a high number of projections which may harm the cellulose. We were able to reduce the dose by a factor of at least 6.67 compared to the high dose scan while keeping the writings visible.

In future, we want to find the best scan parameters and trajectory for the 3-D X-ray CT scan. We assume that this will further increase the image quality of the reconstruction algorithms and the applied dose might be reduced even further. Also the parameters of the reconstruction algorithms may have to be adapted for different trajectories and scan parameters. Due to the limitation of the used X-ray system, we only performed a scan of a small book ($4 \times 4\ cm$) so that the results have to be validated for larger books. Now that we showed that we can reduce the applied dose to a minimum, we want to perform tests with real historical books that can not be opened anymore.

Acknowledgements

We gratefully acknowledge the support of NVIDIA Corporation with the donation of the Titan Xp GPU used for this research.

References

[1] A. Redo-Sanchez, B. Heshmat, A. Aghasi, S. Naqvi, M. Zhang, J. Romberg, and R. Raskar, "Terahertz Time-gated Spectral Imaging for Content Extraction Through Layered Structures", Nature Communications 7, pp. 12665, 2016.

[2] O. Hahn, W. Malzer, B. Kanngiesser, and B. Beckhoff, "Characterization of Iron-Gall Inks in Historical Manuscripts and Music Compositions Using X-ray Fluorescence Spectrometry", X-Ray Spectrometry 33.4, pp. 234-239, 2004.

[3] D. Stromer, V. Christlein, G. Anton, P. Kugler and A. Maier, "3-D Reconstruction of Historical Documents Using an X-Ray C-Arm CT System", Proceedings of the 31th Conference on Image and Vision Computing New Zealand 2016, 2017.

[4] D. Stromer, T. Schoen, W. Holub, and A. Maier, "3-D Reconstruction of Iron Gall Ink Writings", Proceedings of the 7th Conference on Industrial Computed Tomography (iCT 2017), pp. 136-137, 2017.

[5] V. Mocella, E. Brun, C. Ferrero, and D. Delattre, "Revealing Letters in Rolled Herculaneum Papyri by X-ray Phase-contrast Imaging", Nature Communications 6, pp. 5895, 2015.

[6] A. Charlesby, "The Degradation of Cellulose by Ionizing Radiation", Journal of Polymer Science Part A: Polymer Chemistry 15(79), pp. 263-270, 1955.

[7] F. Albertin, A. Patera, I. Jerjen, S. Hartmann, E. Peccenini, F. Kaplan, M. Stampanoni, R. Kaufmann, and G. Margaritondo, "Virtual Reading of a Large Ancient Handwritten Science Book", Microchemical Journal 125, pp. 185-189, 2016.

[8] A. Maier, H. G. Hofmann, C. Schwemmer, J. Hornegger, A. Keil and R. Fahrig. "Fast Simulation of X-ray Projections of Spline-based Surfaces Using an Append Buffer", Physics in Medicine and Biology 57(19), pp. 6193, 2012.

[9] D.L. Parker, "Optimal Short Scan Convolution Reconstruction for Fan Beam CT", Medical Physics 9.2, pp. 254-257, 1982.

[10] F. Noo, M. Defrise, R. Clackdoyle, and H. Kudo, "Image Reconstruction from Fan-Beam Projections on Less than a Short Scan", Physics in Medicine and Biology 47(14), pp. 2525, 2002.

[11] L.A. Feldkamp, L.C. Davis, and J.W. Kress, "Practical Cone-beam Algorithm", JOSA A 1(6), pp. 612-619, 1984.

[12] H. K. Tuy, "An Inversion Formula for Cone-Beam Reconstruction", SIAM Journal on Applied Mathematics 43(3), pp. 546–552, 1983.

[13] J. Thibault, K. D. Sauer, C. A. Bouman, and J. Hsieh, "A Threedimensional Statistical Approach to Improved Image Quality for Multislice Helical CT", Medical physics 34(11), pp. 4526–4544, 2007.

[14] A.H. Andersen, and A.C. Kak, "Simultaneous Algebraic Reconstruction Technique (SART): A Superior Implementation of the ART Algorithm", Ultrasonic imaging 6(1), pp. 81-94, 1984.

[15] B. Keck, H. Hofmann, H. Scherl, M. Kowarschik, and J. Hornegger, "GPU-Accelerated SART Reconstruction Using the CUDA Programming Environment", Proc. SPIE. Vol. 7258, pp. 72582B, 2009.

[16] W. Zbijewski, and F. J. Beekman, "Fbp Initialization for Transition Artifacts Reduction in Statistical X-ray CT Reconstruction", Nuclear Science Symposium Conference Record, 2003 IEEE, volume 4, pp. 2970–2972, 2003.

[17] I. A. Elbakri, and J. A. Fessler, "Statistical Image Reconstruction for Polyenergetic X-ray Computed Tomography", IEEE Transactions on Medical Imaging 21.2, pp. 89-99, 2002.

[18] J. Chen, M. Wu, and Y. Yao, "Accelerating CT Iterative Reconstruction Using ADMM and Nesterov's Methods", 2014.

[19] R. Gordon, R. Bender, and G. T. Herman, "Algebraic Reconstruction Techniques (ART) for Three-dimensional Electron Microscopy and X-ray Photography", Journal of Theoretical Biology 29.3, pp. 471IN1477-476IN2481, 1970.

[20] J. Tang, B. E. Nett, and G.-H. Chen, "Performance Comparison Between Total Variation (TV)-based Compressed Sensing and Statistical Iterative Reconstruction Algorithms", Phys. Med. Biol. 54 (19), pp. 5781–5804, 2009.

[21] H. Wu, A. Maier, R. Fahrig, and J. Hornegger, "Spatial-temporal Total Variation Regularization (STTVR) for 4D-CT Reconstruction", Proc of SPIE 8313, 2012.

[22] E.J. Candès, J. Romberg, and T. Tao, "Robust Uncertainty Principles: Exact Signal Reconstruction from Highly Incomplete Frequency Information", IEEE Trans Inf Theory 52(2), pp. 489–509, 2006.

[23] Y. Huang, O. Taubmann, X. Huang, V. Haase, G. Lauritsch, and A. Maier, "A New Weighted Anisotropic Total Variation Algorithm for Limited Angle Tomography", 2016 IEEE 13th International Symposium on Biomedical Imaging (ISBI), IEEE, 2016.

[24] A. Maier, H.G. Hofmann, M. Berger, P. Fischer, C. Schwemmer, H. Wu, K. Müller, J. Hornegger, J.-H. Choi, and C. Riess, "CONRAD - A Software Framework for Cone-beam Imaging in Radiology", Medical Physics 40(11), pp. 111914, 2013.

[25] D. Stromer, V. Christlein, T. Schoen, W. Holub, and A. Maier, "Fast, Robust and Efficient Extraction of Book Pages from a 3-D X-ray CT Volume", Proceedings of the 14th International Meeting on Fully Three-Dimensional Image Reconstruction in Radiology and Nuclear Medicine, pp. 401-404, 2017.

[26] D. Stromer, V. Christlein, T. Schoen, W. Holub, and A. Maier, "Browsing Through Closed Books: Fully Automatic Book Page Extraction from a 3-D X-ray CT Volume", The 14th IAPR International Conference on Document Analysis and Recognition (ICDAR2017), pp. 224-229, 2017.